

# Noise-driven current reversal and stabilization in the tilted ratchet potential subject to tempered stable Lévy noise

Mathew L. Zuparic and Alexander C. Kalloniatis

*Defence Science and Technology Group, Canberra 2600, Australia*

Dale O. Roberts

*Australian National University, ACT Canberra 2601, Australia*

(Received 27 June 2017; published 13 November 2017)

We consider motion of a particle in a one-dimensional tilted ratchet potential subject to two-sided tempered stable Lévy noise characterized by strength  $\Omega$ , fractional index  $\alpha$ , skew  $\theta$ , and tempering  $\lambda$ . We derive analytic solutions to the corresponding Fokker-Planck Lévy equations for the probability density. Due to the periodicity of the potential, we carry out reduction to a compact domain and solve for the analog of steady-state solutions which we represent as wrapped probability density functions. By solving for the expected value of the current associated with the particle motion, we are able to determine thresholds for metastability of the system, namely when the particle stabilizes in a well of the potential and when the particle is in motion, for example as a consequence of the tilt of the potential. Because the noise may be asymmetric, we examine the relationship between skew of the noise and the tilt of the potential. With tempering, we find two remarkable regimes where the current may be reversed in a direction opposite to the tilt or where the particle may be stabilized in a well in circumstances where deterministically it should flow with the tilt.

DOI: [10.1103/PhysRevE.96.052116](https://doi.org/10.1103/PhysRevE.96.052116)

## I. INTRODUCTION

The impact of stochastic driving in nonlinear systems [1] is significant in diverse physical, chemical, and biological systems; we would also include here social systems for reasons to be given soon. For all the sophistication of these models, some features are common: a potential energy landscape with a tilt, or bias, superimposed with some form of periodicity in the distributions of local minima. These are known as tilted ratchet potentials because of the behavior that, under metastable circumstances, a particle may drift down the tilt but temporarily “catch” in the periodically occurring wells [2]. Many works have addressed Gaussian or Brownian noise in such potentials, or analogous forms such as “washboard” potentials [3,4], and multidimensional forms of these [5]. However, more general forms of noise, particularly with jumps drawn from heavy tails [6] are now topical in the literature, for example spatially stable Lévy noise [7,8] and tempered stable Lévy noise [9–13]. Such concepts have led to the study of so-called fractional (or super)diffusion [14–16]. There is a long history of applications to more standard one-dimensional systems [17–22]. Such non-Gaussian noise models have been applied to ratchet potentials in the absence of tilt [23]. In this paper we extend these analyses to the case of nonzero tilt.

The signature behaviors of interest in stochastic tilted ratchets [3,4,24] are those of current stabilization (where the particle may be localized in a well under the influence of the noise when deterministically it would seek to roll down the tilt) and current reversal (where the particle is driven against the tilt by the noise). These phenomena form a subset of nonlinear collective behaviors alongside stochastically driven resonance [25,26] and synchronization [27]. Given the importance of noise characterized by jumps and heavy tails in diverse contexts [28] such as the fluid properties of plasmas [29,30], finance [31,32], and brain waves [33], the application of this to the collective phenomena of tilted ratchets is evident. Already

in the presence of periodic potentials under tempered stable noise, current reversal has been observed [23]. In this paper we explore the role in this phenomenon of the tilt (which should naturally inhibit current reversal) in the vicinity of the deterministic threshold for current flow.

Our interest in this problem arises from a quite different problem, that of synchronization on networks as exemplified in the stylized Kuramoto model [34]. First, the property of metastability for the Kuramoto model on ring graphs subject to weak Gaussian noise has been identified [35]. This uses the approach to stochastic metastability of Freidlin-Wentzell (FW) theory [36]. Second, the Kuramoto model close to the synchronization threshold maps to a tilted ratchet potential; some of us have explored this property for a generalization of the Kuramoto model for two populations on separate networks [37] and subject to Gaussian noise [38], which may be seen as a representation of competitive social or organizational processes. Finally, some of us have begun explorations of the ordinary Kuramoto model subject to stable [39] and tempered stable noise [40]—with hints at stochastic synchronization there as well.

The paper is structured as follows. In the next section we set up the tempered stable stochastic system, first using the fractional Langevin formalism and then the Fokker-Planck formalism. We then discuss the reduction procedure in light of the periodic structure of the potential, using the Gaussian case as an example. We then present the main results showing the solution to the reduced Fokker-Planck probability density and associated expected value of the current associated with the particle; in this we use a little-known representation of the solutions as “wrapped probability densities.” We examine these under variations of parameters such as the fractional  $\alpha$ , the tilt and the tempering of the noise. Here we identify the regimes of current reversal and stabilization. The paper concludes with prospects for future work.

## II. TEMPERED-FRACTIONAL-FOKKER-PLANCK EQUATIONS IN RATCHET POTENTIALS

We present here the formulation of the problem to be solved. The focus is on certain types of stochastic processes in ratchet potentials. These are potentials that involve *tilted periodic functions*. For this work we use a ratchet potential of the form

$$V(x) = -\mu x - \gamma \cos(x - \rho), \quad \rho \in (-\pi, \pi], \quad (1)$$

where  $\mu \in \mathbb{R}$  and  $\gamma \in \mathbb{R}$  are referred to as the *tilt* and *amplitude* respectively. Equation (1) is commonly referred to as a *tilted periodic ratchet* [1,2]. The potential has two important features. The first is the periodicity  $V'(x) = V'(x + 2\pi)$ . The second is given by the sign of the quantity

$$\mathcal{K} = \gamma^2 - \mu^2, \quad (2)$$

which encapsulates the interplay between the tilt and the amplitude. Specifically, if  $\mathcal{K} > 0$  then  $V(x)$  contains a series of local minima (*stable fixed points*) at  $x = \rho + \sin^{-1}(\mu/\gamma) \bmod 2\pi$ , and a series of local maxima (*unstable fixed points*) at  $x = \pi + \rho - \sin^{-1}(\mu/\gamma) \bmod 2\pi$ . If  $\mathcal{K} = 0$  then the maxima and minima collapse into each other and form a series of inflection points (*unstable fixed points*). Last, if  $\mathcal{K} < 0$  then  $V(x)$  becomes an entirely monotonic function with no inflection points, namely no stationary points.

These properties completely govern the behavior of the deterministic system  $\dot{x} = -V'(x)$ , namely the circumstances for which stationary behavior may be attained ( $\mathcal{K} > 0$ , suspension in a potential well) and what forms of nonstationary behavior are allowed ( $\mathcal{K} < 0$ , “rolling” down the tilt). These behaviors are encoded in the deterministic solution which takes the form [37]

$$x(t) = \rho + 2 \arctan \left\{ \frac{|\gamma| - \sqrt{\mathcal{K}} \tanh\left(\frac{c-t}{2}\sqrt{\mathcal{K}}\right)}{|\mu|} \right\}, \quad (3)$$

with  $c$  an integration constant. The impact of Gaussian noise on this was explored in Ref. [38]. We now wish to see how non-Gaussian stochastic processes change this behavior.

### A. Fractional Langevin equations

We generalize the deterministic system to a Langevin equation combining deterministic and non-Gaussian stochastic dynamics written in stochastic differential notation:

$$dx(t) = -V'(x(t))dt + dL^{\alpha,\theta,\lambda}(t), \quad (4)$$

where  $L^{\alpha,\theta,\lambda}(t)$  is taken to be a *tempered stable* process, given by parameters that describe, respectively, the strength of the power law (or “fractional index”) in the noise tail, the asymmetry or skew of the noise, and the tempering of the tail. As described, for example, in Ref. [41], and clarified further below, the parameters are constrained in the following way:  $\alpha \in (0, 1) \cup (1, 2]$  arising from a stable Lévy process,  $\theta \in [-1, 1]$  is the asymmetry, and  $\lambda \in (0, \infty)$  for the tempering parameter for the heavy tails. For  $\alpha = 2$ , the Lévy noise term in Eq. (4) becomes Gaussian. These parameters describe the tempered-fractional diffusion process, defined in the following.

### B. Tempered-fractional diffusion

The probability density  $\mathcal{P}(x, t)$  associated with the tempered-stable Lévy process  $L^{\alpha,\theta,\lambda}(t)$  in Eq. (4) obeys the following so-called tempered-fractional Fokker-Planck equation (TFFP) [42]

$$\begin{aligned} \frac{\partial}{\partial t} \mathcal{P}(x, t) &= \left\{ \Omega \partial_x^{\alpha,\theta,\lambda} + \frac{\partial}{\partial x} V'(x) \right\} \mathcal{P}(x, t) \\ \mathcal{P}(x, 0) &= \delta(x - y), \end{aligned} \quad (5)$$

where  $\Omega \in \mathbb{R}_+$  is the diffusivity and the operator  $\partial_x^{\alpha,\theta,\lambda}$  is the tempered-fractional-diffusion operator, given explicitly by [23]

$$\partial_x^{\alpha,\theta,\lambda} = \mathcal{D}_x^{\alpha,\theta,\lambda} + v^{\alpha,\theta,\lambda} \frac{\partial}{\partial x} + v^{\alpha,\lambda}. \quad (6)$$

Here  $v^{\alpha,\theta,\lambda}$  and  $v^{\alpha,\lambda}$  are so-called “induced” drift and source-sink terms given by

$$v^{\alpha,\theta,\lambda} = \begin{cases} 0, & \alpha \in (0, 1) \\ \frac{\alpha\theta\lambda^{\alpha-1}}{|\cos(\pi\alpha/2)|}, & \alpha \in (1, 2) \end{cases}, \quad v^{\alpha,\lambda} = \frac{\lambda^\alpha}{\cos(\pi\alpha/2)}. \quad (7)$$

The operator  $\mathcal{D}_x^{\alpha,\theta,\lambda}$  is the  $\lambda$ -truncated fractional derivative of order  $\alpha$ , given by

$$\mathcal{D}_x^{\alpha,\theta,\lambda} = l(\theta)e^{-\lambda x} {}_{-\infty}D_x^\alpha e^{\lambda x} - r(\theta)e^{\lambda x} {}_x D_\infty^\alpha e^{-\lambda x}, \quad (8)$$

where the operators  ${}_{-\infty}D_x^\alpha$  and  ${}_x D_\infty^\alpha$  are the Riemann-Liouville derivatives [43]. Both operators have the following form in Fourier space [44,45]:

$$\begin{aligned} \mathcal{F}[e^{-\lambda x} {}_{-\infty}D_x^\alpha e^{\lambda x} f(x)] &= (\lambda - ik)^\alpha \widehat{f}(k), \\ \mathcal{F}[e^{\lambda x} {}_x D_\infty^\alpha e^{-\lambda x} f(x)] &= (\lambda + ik)^\alpha \widehat{f}(k), \end{aligned} \quad (9)$$

where our convention for the Fourier transform is

$$\begin{aligned} \mathcal{F}[f(x)] &= \int_{-\infty}^{\infty} dx e^{ikx} f(x) = \widehat{f}(k), \\ \mathcal{F}^{-1}[\widehat{f}(k)] &= \int_{-\infty}^{\infty} \frac{dk}{2\pi} e^{-ikx} \widehat{f}(k) = f(x). \end{aligned} \quad (10)$$

Finally, for definitional purposes, the weighting factors

$$l(\theta) = \frac{\theta - 1}{2 \cos(\pi\alpha/2)}, \quad r(\theta) = \frac{\theta + 1}{2 \cos(\pi\alpha/2)} \quad (11)$$

give the asymmetry imposed on each of the Riemann-Liouville derivatives. Taking the Fourier transform of the fractional derivative  $\partial_x^{\alpha,\theta,\lambda}$  we obtain

$$\begin{aligned} \mathcal{F}[\partial_x^{\alpha,\theta,\lambda} f(x)] &= \{l(\theta)(\lambda - ik)^\alpha - r(\theta)(\lambda + ik)^\alpha - ikv^{\alpha,\theta,\lambda} \\ &\quad + v^{\alpha,\lambda}\} \widehat{f}(k) = \Lambda(k) \widehat{f}(k), \end{aligned} \quad (12)$$

where  $\Lambda(k)$  is the logarithm of the characteristic function of the tempered stable Lévy process.

For the stable limit,  $\lambda \rightarrow 0$ , Eq. (5) arises from a continuous time random walk (CTRW) process (in the absence of waiting times), as shown in Ref. [14]; in this limit the process is governed by the characteristic function as given in the Lévy-Khinchine law [46]. The generalization to the tempered case is given in Ref. [42], where the dynamical equation (5) is a special case of a macroscopic transport equation in the continuum “fluid limit” of a CTRW for a specific case of a density describing the jump distribution of the random

walkers. As [42] argues, the generalization of the problem to an external potential is achieved by adding the potential, indeed as considered in Ref. [23].

The key property of tempered stable noise that makes it attractive lies in the moments of the density for CTRW jumps. For  $\lambda = 0$ , the stable process only admits finite moments of order  $n < \alpha$ . Thus, for fractional  $\alpha \in (1, 2]$  only first order moments exist. This means that one cannot fit a model to a *finite* dataset (all empirical moments are finite). Tempering with  $\lambda \neq 0$ , renders all moments finite while retaining the property of the heavy tail [12,23,41,42].

**C. Illustrative example: Gaussian limit**

In order to proceed with the general TFFP equation with the tilted ratchet potential, we first briefly detail the Gaussian limit case, namely

$$\frac{\partial}{\partial t} \mathcal{P}(x, t) = \left\{ \Omega \frac{\partial^2}{\partial x^2} + \frac{\partial}{\partial x} V'(x) \right\} \mathcal{P}(x, t), \quad (13)$$

as its relatively simple explanation of solution allows for greater intuition when we consider the more complicated fractional case. As well as the defining equation (13), we are also concerned with the *probability current*  $\mathcal{J}(x, t)$ , defined by the following probability conservation expression:

$$\begin{aligned} \frac{\partial}{\partial t} \mathcal{P}(x, t) + \frac{\partial}{\partial x} \mathcal{J}(x, t) &= 0 \\ \Rightarrow \mathcal{J}(x, t) &= - \left\{ \Omega \frac{\partial}{\partial x} + V'(x) \right\} \mathcal{P}(x, t). \end{aligned} \quad (14)$$

As explained in Ref. [1] and references therein, one finds a non-normalizable density when following the usual procedure for a steady-state solution: solving the Pearson equation for the steady-state density  $\mathcal{P}_{st}(x)$ , namely setting  $\frac{\partial}{\partial t} \mathcal{P}(x, t) = 0$  in Eq. (13), and applying the vanishing boundary condition  $\mathcal{P}_{st}(x) \rightarrow 0$  at the natural boundaries  $x \rightarrow \pm\infty$ . This is due to the periodicity of the ratchet potential and its *metastability* in the presence of noise [35,36,47]. In order to circumvent this phenomenon, we restrict the support of  $x$  to  $\mathbb{S}^1$  by constructing the so-called *reduced density*  $\mathcal{P}^{(r)}(x, t)$  and *reduced probability current*  $\mathcal{J}^{(r)}(x, t)$  through

$$\begin{aligned} \mathcal{P}^{(r)}(x, t) &\equiv \sum_{n=-\infty}^{\infty} \mathcal{P}(x + 2\pi n, t), \\ \mathcal{J}^{(r)}(x, t) &\equiv \sum_{n=-\infty}^{\infty} \mathcal{J}(x + 2\pi n, t). \end{aligned} \quad (15)$$

Due to the linearity of the Fokker-Planck equation, the reduced density and reduced probability current also obey Eqs. (13) and (14) respectively, but with the new boundary and normalization conditions

$$\mathcal{P}^{(r)}(-\pi, t) = \mathcal{P}^{(r)}(\pi, t), \quad \int_{-\pi}^{\pi} dx \mathcal{P}^{(r)}(x, t) = 1. \quad (16)$$

The reduced steady-state density is then given by [48]

$$\mathcal{P}_{st}^{(r)}(x) = \frac{\sinh\left(\frac{\pi\mu}{\Omega}\right) e^{-V(x)/\Omega} \int_x^{x+2\pi} d\varphi e^{V(\varphi)/\Omega}}{2\pi^2 \left| I_{i\mu}\left(\frac{\gamma}{\Omega}\right) \right|^2 (1 - e^{-2\pi\mu/\Omega})}, \quad (17)$$

where  $I_{i\mu}$  is the modified Bessel function of imaginary order.

Additionally, the corresponding average velocity  $\langle \dot{x} \rangle$ , which may assume nonzero values as a consequence of the metastability and the tilt of the potential  $\mu$ , is given by [48]

$$\langle \dot{x} \rangle = \frac{d}{dt} \langle x \rangle = \int_{-\pi}^{\pi} dx \mathcal{J}_{st}^{(r)}(x) = \frac{\Omega \sinh\left(\frac{\pi\mu}{\Omega}\right)}{\pi \left| I_{i\mu}\left(\frac{\gamma}{\Omega}\right) \right|^2}. \quad (18)$$

Note that, trivially, for Gaussian noise there is zero average velocity in the absence of tilt:  $\langle \dot{x} \rangle = 0$  if  $\mu = 0$ .

Figure 1 gives examples of Eq. (17) (insets) and Eq. (18) (main figure) where we have fixed the amplitude  $\gamma = 1$ ; thus deterministically, the point of instability  $\mathcal{K} = 0$  occurs when  $\mu = \pm 1$  from Eq. (2) so for  $\mu = (-1, 1)$   $\dot{x}(t \rightarrow \infty) = 0$ . We also choose the offset  $\rho = -1.5$ . The main part of Fig. 1 shows the average velocity  $\langle \dot{x} \rangle$  as a function of the tilt  $\mu$ . We see that for weak noise,  $\Omega = 10^{-3}$ , the current is vanishing inside the interval  $(-1, 1)$  and increases positively, respectively negatively, for  $\mu > 1$ , respectively  $< -1$ . The particle “rolls” in the direction of the tilt. For increasing  $\Omega$  in the Gaussian noise, the current assumes nonzero values inside the region where deterministically it should vanish: the noise generates tails that allow the particle to “spill” outside the potential wells giving a nonvanishing probability that the particle rolls with the tilt when deterministically it should be stable; hence the particle is metastable.

We also examine these same properties through the probability density solutions of the Gaussian Fokker-Planck equation as insets in Fig. 1. The left-most inset provides a case with stable fixed points ( $\gamma = 1, \mu = 0.99$ ) and the right-most inset details a case with no fixed points ( $\gamma = 1, \mu = 1.01$ ). Both insets are presented as so-called “wrapped probability density functions” (see for example [49]), namely a parametric plot where

$$\begin{aligned} \{x, y\} &= \left\{ (1 + \mathcal{P}_{st}^{(r)}(\phi)) \cos \phi, (1 + \mathcal{P}_{st}^{(r)}(\phi)) \sin \phi \right\}, \\ &\text{for } \phi \in \mathbb{S}^1. \end{aligned} \quad (19)$$

Note that in such plots the convention is that the positive horizontal axis represents  $\phi = 0$  (which would correspond to the vertical axis for a density on the real line); peaks located clockwise from this are in the positive direction and those anticlockwise are in the negative.

For the leftmost inset in Fig. 1, for small  $\Omega$  we see that the density is approximately concentrated at the deterministic position of the stable fixed point [ $\phi = \rho + \sin^{-1}(\mu/\gamma) \approx -0.07$ , and thus the peak is oriented slightly below the horizontal axis]. Moreover, as  $\Omega$  increases we see that the probability density begins to smear around the circle, losing any discernible features after  $\Omega = 1$ . This displays the phenomenon of metastability in the wrapped densities: the particle is rolling with some probability so the probability density is distributed around the entire circle.

The narrative is similar for the right-most inset, except the relative heights of the densities is significantly less—indicating that even for the weakest noise there is a nonvanishing probability that the particle is at other points around the circle because deterministically the particle will roll for  $\mu > 1$ . Further increases in  $\Omega$  distend the peak until it is uniformly distributed around the circle.

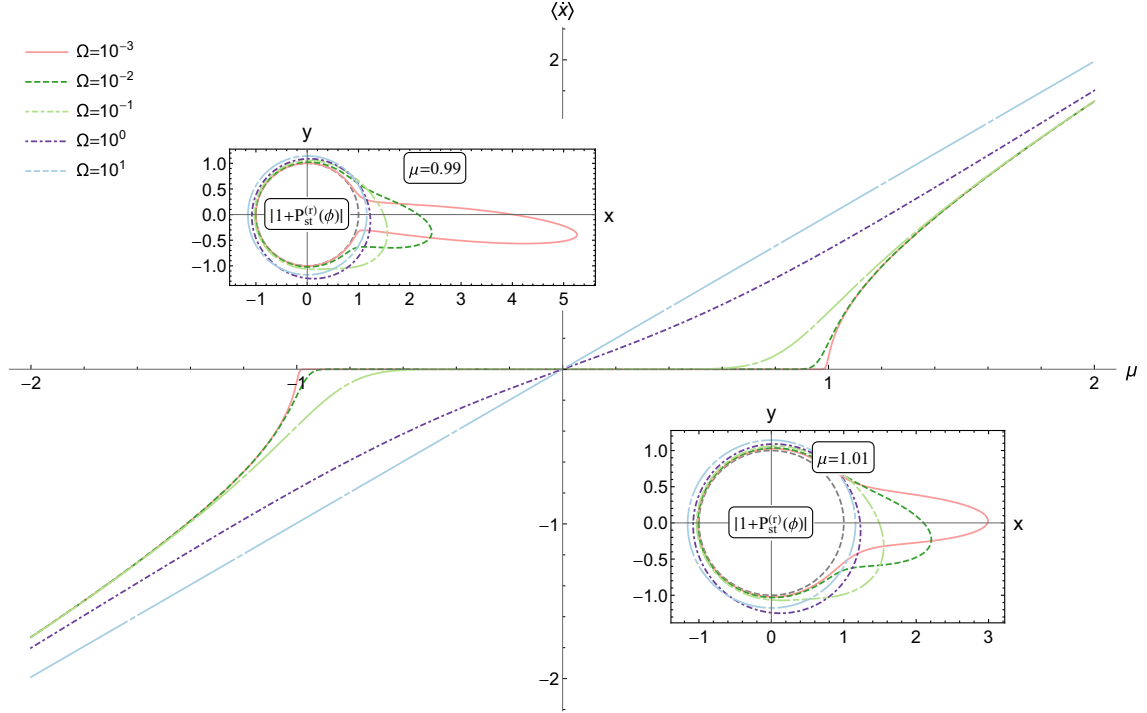


FIG. 1. Examples of Eq. (17) (insets) and Eq. (18) (main) for  $\rho = -1.5$  and  $\gamma = 1$  and various values of the diffusivity  $\Omega$  which governs noise strength. The leftmost inset details a case with stable fixed points in the potential ( $\mu = 0.99$ ), the rightmost inset details a case with no fixed points in the potential ( $\mu = 1.01$ ). Both insets are given as a parametric plot governed by Eq. (19).

The wrapped densities also provide insight into the range of fluctuations. So, for  $\mu = 1.01$  the weakest noise  $\Omega = 10^{-3}$  has a density that is evenly distributed on either side of the horizontal axis, indicating that fluctuations about the average of zero are symmetrically distributed. As  $\Omega$  increases, the bulge moves clockwise around from the horizontal axis indicating that fluctuations are biased in the positive direction—the direction of the tilt. Similar properties are seen for  $\mu = 0.99$  but at stronger values of  $\Omega$ .

### III. ANALYTIC SOLUTION OF THE TFFP EQUATION

#### A. Reduced density

As with the Gaussian case, we expect that the steady-state equivalent of Eq. (5) with vanishing boundary conditions at the natural boundaries  $x \rightarrow \pm\infty$  will be non-normalizable due to metastability. In order to ameliorate this situation we again consider a reduced density defined on  $\mathbb{S}^1$  [Eq. (15)] for the steady-state TFFP equation

$$\left\{ \Omega \partial_x^{\alpha, \theta, \lambda} + \frac{\partial}{\partial x} V'(x) \right\} \mathcal{P}_{st}^{(r)}(x) = 0, \quad (20)$$

with boundary and normalization conditions given by Eq. (16).

Taking the Fourier transform of Eq. (20) we obtain

$$\begin{aligned} & \{\Omega \Lambda(k) + ik\mu\} \widehat{\mathcal{P}}_{st}^{(r)}(k) \\ &= \frac{k\gamma}{2} \{e^{-i\rho} \widehat{\mathcal{P}}_{st}^{(r)}(k+1) - e^{i\rho} \widehat{\mathcal{P}}_{st}^{(r)}(k-1)\} \\ \Rightarrow & \widehat{\mathcal{Q}}(k+1) = -f_k \widehat{\mathcal{Q}}(k) + \widehat{\mathcal{Q}}(k-1), \end{aligned} \quad (21)$$

where  $\widehat{\mathcal{Q}}(k) = e^{-ik\rho} \widehat{\mathcal{P}}_{st}^{(r)}(k)$  and

$$f_k = -\frac{2}{k\gamma} \{\Omega \Lambda(k) + ik\mu\}. \quad (22)$$

Equation (21) represents a *linear* three-term recurrence relation defining the coefficients in the Fourier expansion.

Because of the periodic boundary conditions of  $\mathcal{P}_{st}^{(r)}(x)$  on the finite interval, the Fourier variable  $k$  only takes discrete values. Specifically,

$$\begin{aligned} \mathcal{F}[\mathcal{P}_{st}^{(r)}(x)] &= \sum_{n=-\infty}^{\infty} \mathcal{F}[\mathcal{P}_{st}(x + 2\pi n)] \\ &= \widehat{\mathcal{P}}_{st}(k) \sum_{n=-\infty}^{\infty} e^{-i2\pi nk} \\ &= \widehat{\mathcal{P}}_{st}(k) \sum_{m=-\infty}^{\infty} \delta(k - m). \end{aligned}$$

Thus we need to solve the three term recurrence relation for coefficients  $\widehat{\mathcal{Q}}(k)$  in Eq. (21) for  $k \in \{\dots, -1, 0, 1, \dots\}$ . Doing so, we can then construct the probability density via the discrete inverse Fourier transform

$$\mathcal{P}_{st}^{(r)}(x) = \frac{1}{2\pi} \left\{ \widehat{\mathcal{Q}}(0) + 2\text{Re} \sum_{n=1}^{\infty} e^{-in(x-\rho)} \widehat{\mathcal{Q}}(n) \right\}, \quad (23)$$

where  $\widehat{\mathcal{Q}}(0) = 1$  from the normalization condition in Eq. (16).

Following Chap. 9 of [50], applying the transformations

$$S_{k+1} = \frac{\widehat{\mathcal{Q}}(k+1)}{\widehat{\mathcal{Q}}(k)}$$

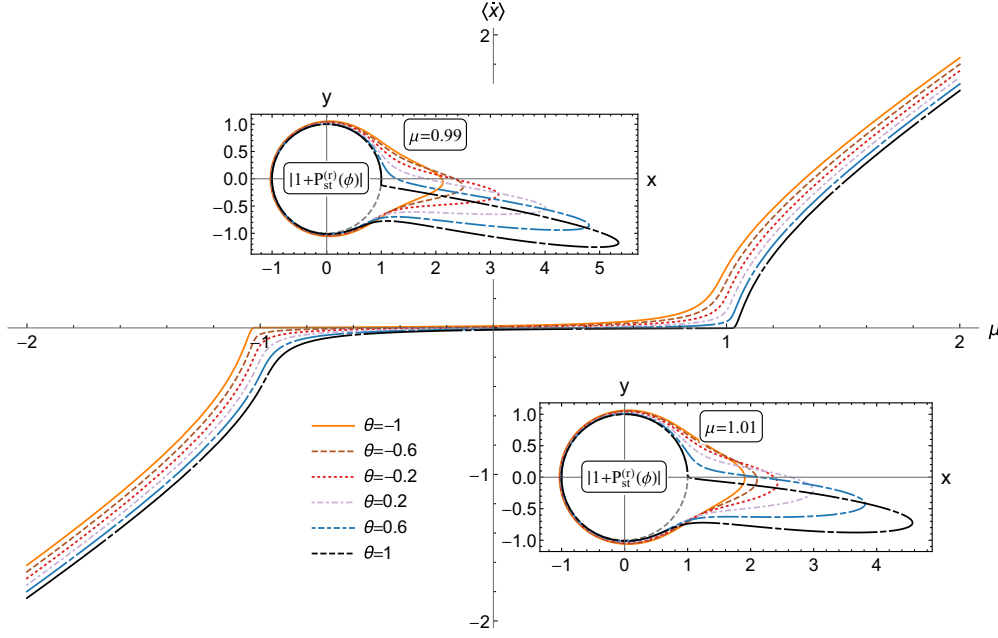


FIG. 2. Examples of Eq. (23) (insets) and Eq. (27) (main) for  $\rho = -1.5$ ,  $\gamma = 1$ ,  $\alpha = 0.5$ ,  $\lambda = 0.5$ ,  $\Omega = 0.1$  and various values of the asymmetry  $\theta$ . The left-most inset details a case with stable fixed points in the potential ( $\mu = 0.99$ ), the right-most inset details a case with no fixed points in the potential ( $\mu = 1.01$ ). Both insets are given as a parametric plot governed by Eq. (19).

the linear three term recurrence relation in Eq. (21) becomes the following *nonlinear* two term recurrence relation:

$$S_k = \frac{1}{f_k + S_{k+1}}, \quad (24)$$

which can be solved iteratively using continued fractions

$$S_k = \frac{1}{f_k + \frac{1}{f_{k+1} + S_{k+2}}} = \frac{1}{f_k + \frac{1}{f_{k+1} + \frac{1}{f_{k+2} + \frac{1}{\ddots}}}}$$

Moreover, applying the notation

$$\mathbb{K}_{j=1}^m(a_j : b_j) = \frac{a_1}{b_1 + \frac{a_2}{b_2 + \frac{a_3}{\ddots + \frac{a_m}{b_m}}}}$$

$S_k$  can be conveniently expressed by

$$S_k = \mathbb{K}_{j=k}^{\infty}(1 : f_j). \quad (25)$$

Calculating the expressions for  $\{S_k, S_{k-1}, \dots, S_2, S_1\}$ , we may then reconstruct the corresponding  $\widehat{Q}(k)$  using

$$\widehat{Q}(k) = S_k S_{k-1} \dots S_2 S_1 \widehat{Q}(0) \quad (26)$$

for insertion into Eq. (23). Thus Eq. (23) with coefficients given by Eq. (26) is the solution to the TFFP equation, equivalent to Eq. (17) for Gaussian noise.

For numerical calculations of the reduced density we truncate the number of terms in Eq. (23) at  $n = 1000$ . Moreover,

for the continued fractions  $S_k$  in Eq. (25) that form the density in Eq. (23), we approximate these as  $S_k = \mathbb{K}_{j=k}^p(1 : f_j)$ , where  $k = \{1, \dots, 1000\}$ , and  $p = 2000$ .

## B. Average velocity

Considering the expression for the the average velocity  $\langle \dot{x} \rangle \equiv \frac{d}{dt} \langle x \rangle$  given in Eq. (18) we may perform the following sequence of manipulations to re-express the expected current in terms of the characteristic function for the tempered stable Lévy process:

$$\begin{aligned} \frac{d}{dt} \langle x \rangle &= \frac{d}{dt} \langle x e^{ikx} \rangle|_{k \rightarrow 0} \\ &= \frac{\partial}{\partial t} \left\{ -i \frac{\partial}{\partial k} \widehat{\mathcal{P}}(k, t) \right\} |_{k \rightarrow 0} \\ &= -i \frac{\partial}{\partial k} \left\{ \frac{\partial}{\partial t} \widehat{\mathcal{P}}(k, t) \right\} |_{k \rightarrow 0} \\ &= -i \frac{\partial}{\partial k} \{ \Omega \Lambda(k) \widehat{\mathcal{P}}(k, t) - ik \mathcal{F}[V'(x) \mathcal{P}(x, t)] \} |_{k \rightarrow 0} \\ &= -i \Omega \frac{d}{dk} \Lambda(k) |_{k \rightarrow 0} - \mathcal{F}[V'(x) \mathcal{P}(x, t)] |_{k \rightarrow 0}. \end{aligned}$$

From Eq. (12)

$$-i \Omega \frac{d}{dk} \Lambda(k) |_{k \rightarrow 0} = \begin{cases} -\frac{\Omega \alpha \theta \lambda^{\alpha-1}}{\cos(\frac{\pi \alpha}{2})} & 0 < \alpha < 1 \\ 0 & 1 < \alpha < 2 \end{cases}$$

and from Eqs. (1) and (23)

$$-\mathcal{F}[V'(x) \mathcal{P}(x, t)] |_{k \rightarrow 0} = \mu - 2\pi \gamma \text{Im} \{ \widehat{Q}(1) \}.$$

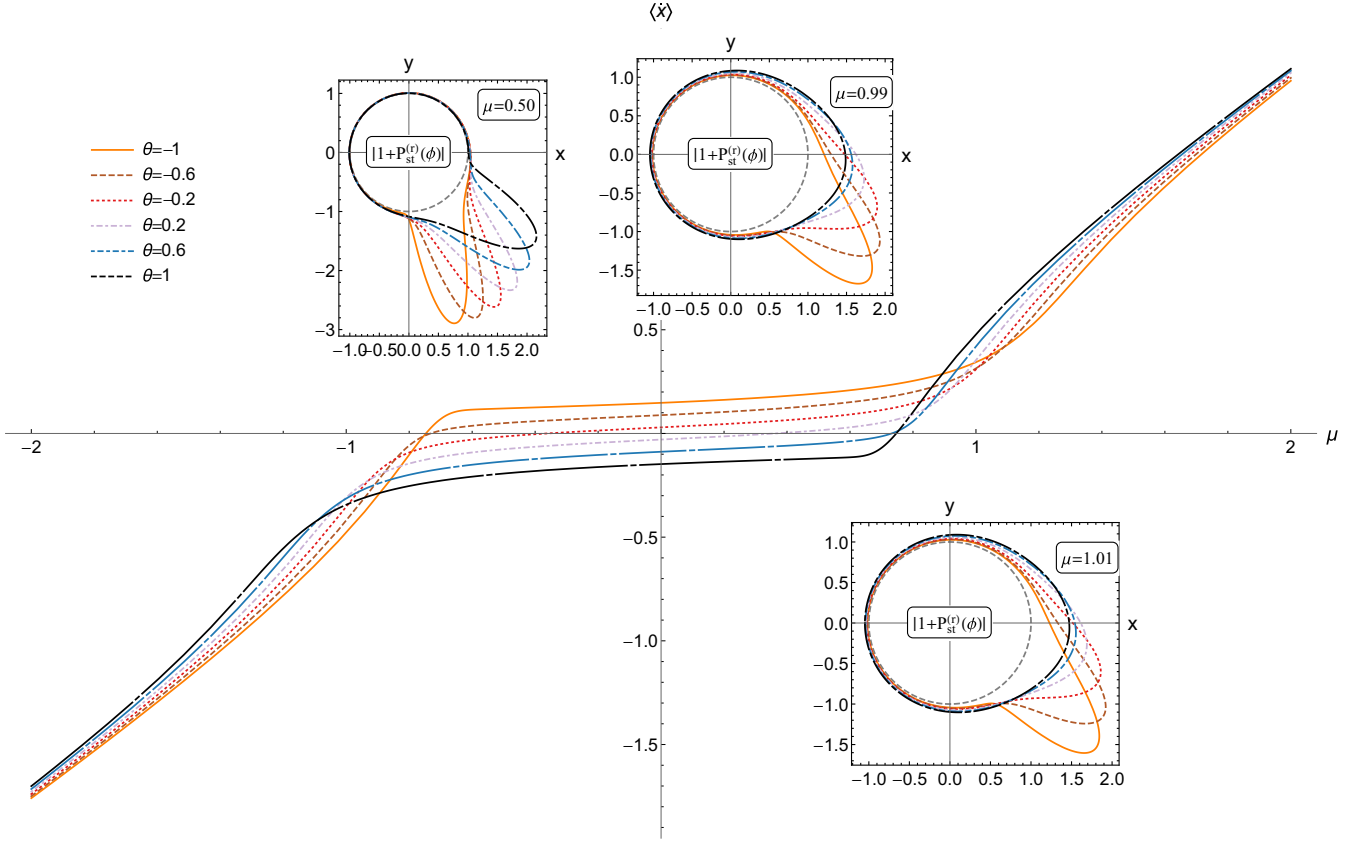


FIG. 3. Examples of Eq. (23) (insets) and Eq. (27) (main) for  $\rho = -1.5$ ,  $\gamma = 1$ ,  $\alpha = 1.25$ ,  $\lambda = 0.001$ ,  $\Omega = 0.1$  and various values of the asymmetry  $\theta$ . The left-most inset details a case with stable fixed points in the potential ( $\mu = 0.5$ ), the middle inset is  $\mu = 0.99$ , and the right-most inset details a case with no fixed points in the potential ( $\mu = 1.01$ ). The insets are given as a parametric plot governed by Eq. (19).

Hence the expected value of the velocity may be expressed as

$$\langle \dot{x} \rangle = \begin{cases} -\frac{\Omega \alpha \theta \lambda^{\alpha-1}}{\cos(\frac{\pi \alpha}{2})} + \mu - 2\pi \gamma \text{Im}\{\widehat{Q}(1)\} & 0 < \alpha < 1 \\ \mu - 2\pi \gamma \text{Im}\{\widehat{Q}(1)\} & 1 < \alpha < 2. \end{cases} \quad (27)$$

Equation (27) with  $\widehat{Q}(1)$  given by Eq. (26) is the tempered-stable equivalent of Eq. (18) for Gaussian noise.

For the corresponding numerical calculations of the average velocity in Eq. (27), only the first continued fraction coefficient  $\widehat{Q}(1) = S_1 \widehat{Q}(0)$  is involved. For numerical purposes we again truncate  $S_1$  as  $S_1 = \mathbb{K}_{j=1}^p(1 : f_j)$ . For  $\alpha > 1$  we set  $p = 2 \times 10^4$ . However, for  $\alpha < 1$  we find it necessary to set  $p = 4 \times 10^4$  to obtain sufficiently smooth plots of the average velocity.

#### IV. EXAMPLES: CURRENT STABILIZATION AND REVERSAL

As for the Gaussian case, we fix the amplitude  $\gamma = 1$  so that the deterministic threshold for instability is  $\mu = \pm 1$ . We also fix the diffusivity constant at  $\Omega = 0.1$ , where the Gaussian case in Fig. 1 shows diffusion even for  $\mu < 1$  due to metastability, and  $\rho = -1.5$  as before. We first examine the average velocity and wrapped densities for selective values of  $\alpha$  and  $\lambda$ .

With  $\alpha = 0.5$  we expect for the stable noise case ( $\lambda = 0$ ) very heavy tails which will lead to quite diffuse densities. To identify structure we therefore choose for this  $\alpha$  relatively large tempering, namely  $\lambda = 0.5$ . The analog to Fig. 1 is shown in Fig. 2, where again the average velocity is shown as a function of  $\mu$  for different values now of skew  $\theta$ , and insets show the wrapped densities for two the choices of  $\mu$  above and below the threshold  $\mu = 1$ .

The signature feature of Fig. 2 is the behavior around  $\mu = 1$ : we see that for  $\theta = 1$  (black curve) the average velocity is zero for a small range of values  $1 < \mu \leq 1.05$ ; near  $\mu = -1$  the same behavior recurs for  $\theta = -1$ . Once the skew decreases,  $\theta < 1$  for  $1 < \mu \leq 1.05$ , and increases  $\theta > -1$  for  $-1.05 \leq \mu < -1$ , the average velocity becomes nonzero in these narrow regions. In other words, one-sided tempered stable noise antialigned to the tilt may stabilize the particle on average in circumstances where deterministically it should be unstable (namely there is no well). This is *stochastic current stabilization*.

These properties are reflected in the wrapped densities in the inset. The left-most inset of Fig. 2, for  $\mu = 0.99$ , shows strongly peaked densities just as for the Gaussian case. However, the right-most inset with  $\mu = 1.01$  also shows a strongly peaked density for  $\theta = 1$  where the analogous Gaussian case of Fig. 1 shows diffusion around the circle (particularly for the corresponding value of  $\Omega$ ). Observe how

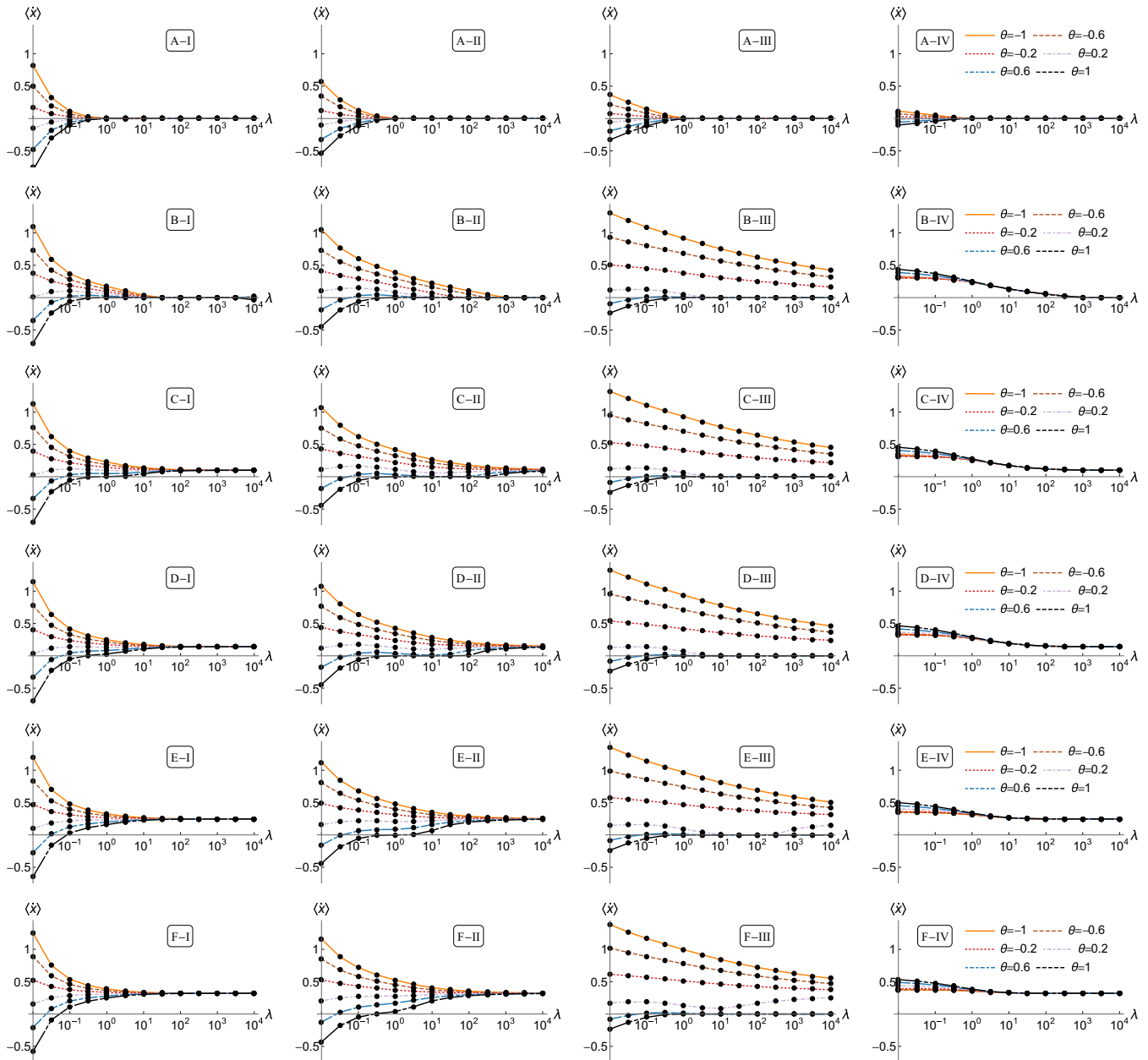


FIG. 4. Examples of Eq. (27) for  $\rho = -1.5$ ,  $\gamma = 1$ ,  $\Omega = 0.1$ . The tempering  $\lambda$  is being varied on the horizontal axis, with various values of the asymmetry  $\theta$ . Down the rows (A-F) the tilt  $\mu$  is varied, with the values  $\mu = \{0.1, 0.995, 1.005, 1.01, 1.03, 1.05\}$  being applied from top to bottom row. Across the columns (I-IV) the fractional power  $\alpha$  is varied, with the values  $\alpha = \{0.25, 0.55, 0.85, 1.25\}$  applied from left-most to right-most column.

for both cases of  $\mu$ , the curve for the one-sided density with  $\theta = 1$  joins the circle sharply on one side (anticlockwise from the peak) and more smoothly on the other (clockwise from the peak). This manifests the skew for this case.

We now chose a contrasting case with  $\alpha = 1.25$ , greater than 1 but still significantly far from Gaussianity, and  $\lambda = 0.001$  which is close to the stable limit. The corresponding average velocity and wrapped densities are shown in Fig. 3, but now for three choices of  $\mu$ . Now for  $-1 < \mu < 1$  the average velocity no longer vanishes in general except for specific values of  $\theta$  at specific values of  $\mu$ ; at such values the skew exactly

balances against the tilt. However, unusually, there are regions where the sign of  $\langle \dot{x} \rangle$  is opposite to that of  $\mu$  for certain ranges of skew  $\theta$ . For example, for  $\theta = 1$  (black curve) and  $0 < \mu < 0.7$ ,  $\langle \dot{x} \rangle < 0$ , the particle is propagating in the negative direction (to the left) even though skew and tilt are positive. For  $\theta = -1$  (orange curve) and  $-0.7 < \mu < 0$ ,  $\langle \dot{x} \rangle > 0$ , so that the particle is propagating in the positive direction (to the right) even though skew and tilt are negative. This is the phenomenon of current reversal.

Examining the wrapped densities, shown in the insets, we see strongly oriented and sharp densities for  $\mu = 0.5$  across

the range of  $\theta$ , while for  $\mu = 0.99, 1.01$  the densities are mostly diffuse for  $\theta > 0$ , most strongly for  $\theta = 1$ . These assist, to a degree, in understanding the counterintuitive current reversal. Specifically, we observe that for the one-sided case  $\theta = -1$  (orange curve) the heavy tail is in the anticlockwise direction while the peak is oriented clockwise from the positive horizontal direction. Recalling that all of the cases of  $\theta$  correspond to the same mean, we observe that the mode of the distribution shifts further and further clockwise from the axis. This indicates that the heavy tail is in the anticlockwise direction (in contrast to the  $\theta = 1$  case). Significantly, for  $\alpha > 1$  the mode of the distribution lies in the opposite direction from the heavy tail [39]. The wrapped densities, particularly with the distortions of plotting on a circle, do not convey well the significance of the heavy tail; in Ref. [39] the role of the tail was best represented through quartile-quartile plots. Nevertheless, in the case of such small tempering given a heavy tail in the negative direction for  $\theta < 0$ , we obtain a probability mass in the positive direction. So there is a dominance of small jumps in the positive direction. Thus, with small tempering and even subject to positive tilt, there is a net drift in the positive direction. The current reversal arises from this. (We only caution that the threshold for this behavior cannot immediately be read off the wrapped density plots since they represent the density of  $x$  rather than the current density.) A similar phenomenon was observed in the Kuramoto model in Ref. [39], a point to which we shall return in the final section.

Having examined two selected cases, we now conduct a more general scan across a range of  $\lambda$  for representative values of  $\alpha$  below and above 1 and different skew values  $\theta$ . This is shown in Fig. 4. These plots should be compared with Fig. 15 in Ref. [23] for tempered stable noise in a (different to ours) ratchet potential without tilt ( $\mu = 0$ ). We choose  $\mu$  quite far from this regime, and scan in the vicinity of  $\mu = 1$ , namely  $0.995 \leq \mu \leq 1.05$  and  $\alpha = 0.25, 0.55, 0.85, 1.25$ . But for some comparison we also provide the result for  $\mu = 0.1$ . As  $\mu > 0$  for all these cases, current reversal corresponds to negative values of  $\langle \dot{x} \rangle$  in these plots.

In fact, we observe that current reversal is a generic feature both below the deterministic threshold of  $\mu = 1$  and above, starting from the top left and scanning across to higher values of  $\alpha$ , and scanning down with increasing increments in  $\mu$ . The case shown in Ref. [23], where they choose  $\alpha = 1.5$  and two values of  $\theta$ , shows a current starting negative for small  $\lambda$ , crossing zero to positive values and then converging to zero; this is hidden in a plot such as panel A-IV in Fig. 4. For larger tilt  $\mu$  such behavior moves to  $\alpha < 1$ . For example, panel B-I shows curves for  $\theta \approx 0.6$  crossing from negative to positive and then converging to zero. This current reversal occurs not only for the most extreme skew  $\theta = 1$  but closer to symmetric noise.

We see that for  $\mu < 1$  and large  $\lambda$  the average velocity tends to zero (top two rows); for  $\mu > 1$  the asymptotic limit is nonzero and positive (third row and below), which corresponds to the deterministic value as tempering suppresses all noise. We also observe that the current reversal ceases above  $\alpha = 1$  in this region of  $\mu$ —recall that in Fig. 3 the reversal occurs for  $\mu < 0.7$ .

Within the regimes of current reversal there are always discrete values where  $\langle \dot{x} \rangle = 0$ . However, we also see for  $\mu > 1$

and  $\alpha < 1$  regimes where the average velocity *vanishes across a continuum* of  $\lambda$  values before increasing and converging to the deterministic limit—this is most distinct in panel C-II. Thus current stabilization may be sustained across a broad range of  $\lambda$  before tempering dampens the noise completely. These demonstrate that current stabilization is linked naturally to current reversal, but the stabilization over a range of  $\lambda$  may not be intuitively expected.

Moving to the lower rows we observe that the range of  $\lambda$  over which stabilization occurs shrinks until it becomes only a discrete case of  $\lambda$  except for pure one-sided noise with  $\theta = 1$ . For the cases in panels E-III and F-III with  $\theta = 1$  the average velocity will converge to its nonzero value at  $\lambda$  values beyond those plotted here.

## V. CONCLUSIONS AND DISCUSSION

We have solved the Fokker-Planck equation for a particle in a one-dimensional tilted ratchet potential under tempered stable Lévy noise and have observed both phenomena of current stabilization and reversal, particularly in regimes where deterministic or Gaussian considerations would show quite different behavior.

The essence of the mechanism is the interplay between probability mass around the mode of the underlying noise distributions and the heavy tails and how it shifts as  $\alpha, \lambda$  are varied. Specifically, for  $\alpha > 1$  the mode is typically in the opposite direction from the tail for asymmetric noise as discussed in Ref. [39]. This leads to a drift in a direction corresponding to the sign of the mode, which manifests as current reversal for the particle in the tilted ratchet. When  $\alpha < 1$ , due to the induced drift through the form of the noise characteristic function, the mode and heavy tails are in the same direction but with increased mass around the mode and heavier tails. Thus, with tempering, both long range and intermediate range jumps are suppressed so that the effective drift may even drop down to zero with increased skew in the noise. Moreover, tempering moderates current reversal until it assumes the form of current stabilization. Thus the particular cases of current reversal in Ref. [23] are a special instance of a phenomenon in the presence of tilt in the potential.

As alluded in the Introduction, for us the interest in this phenomenon arises from our work on the Kuramoto model or related forms. In Refs. [39] and [40] we have observed a phenomenon of oscillators of zero native frequency nevertheless synchronizing to a nonzero net frequency, a drift, that shifts in sign according to the interplay of  $\alpha$  and  $\lambda$ . While general observations of the position of the mode and the heaviness of the tail in those cases provide a heuristic explanation of this phenomenon, we argue that the model solved here may provide a deeper insight into this behavior. Future applications of this idea lie in its exploitation for stochastic control of synchronization phenomena.

## ACKNOWLEDGMENT

A.C.K. was supported through a Chief Defence Scientist Fellowship.

- [1] P. Reimann, Brownian motors: Noisy transport far from equilibrium, *Phys. Rep.* **361**, 57 (2002).
- [2] B. Linder, M. Kostur, and L. Schimansky-Geier, Optimal diffusive transport in a tilted periodic potential, *Fluct. Noise* **1**, R25 (2001).
- [3] D. Hennig, Current control in a tilted washboard potential via time-delayed feedback, *Phys. Rev. E* **79**, 041114 (2009).
- [4] C. Mulhern and D. Hennig, Current reversals of coupled driven and damped particles evolving in a tilted potential landscape, *Phys. Rev. E* **84**, 036202 (2011).
- [5] K. J. Challis and M. W. Jack, Tight-binding approach to overdamped Brownian motion on a multidimensional tilted periodic potential, *Phys. Rev. E* **87**, 052102 (2013).
- [6] A. A. Borovkov and K. A. Borovkov, *Asymptotic Analysis of Random Walks: Heavy-tailed Distributions* (Cambridge University Press, Cambridge, UK, 2008).
- [7] J. M. Chambers, C. L. Mallows, and B. W. Stuck, A Method for Simulating Stable Random Variables, *J. Am. Stat. Assoc.* **71**, 340 (1976).
- [8] M. C. K. Tweedie, in *Statistics: Applications and New Directions: Proc. Indian Statistical Institute Golden Jubilee International Conference*, edited by J. Ghosh and J. Roy (Indian Statistical Institute, Calcutta, 1984), pp. 579–604.
- [9] R. N. Mantegna and H. E. Stanley, Stochastic Process with Ultraslow Convergence to a Gaussian: The Truncated Lévy Flight, *Phys. Rev. Lett.* **73**, 2946 (1994).
- [10] I. Koponen, Analytic approach to the problem of convergence of truncated Lévy flights towards the Gaussian stochastic process, *Phys. Rev. E* **52**, 1197 (1995).
- [11] M. M. Meerschaert and F. Sabzikar, Tempered fractional stable motion, *J. Theor. Probab.* **29**, 681 (2016).
- [12] B. Baeumer and M. M. Meerschaert, Tempered stable Lévy motion and transient super-diffusion, *J. Comput. Appl. Math.* **233**, 2438 (2010).
- [13] J. Gajda and M. Magdziarz, Fokker-Planck equation with tempered  $\alpha$ -stable waiting times: Langevin picture and computer simulation, *Phys. Rev. E* **82**, 011117 (2010).
- [14] R. Metzler and J. Klafter, The random walk's guide to anomalous diffusion: A fractional dynamics approach, *Phys. Rep.* **339**, 1 (2000).
- [15] G. Jumarie, Fractional Brownian motions via random walk in the complex plane and via fractional derivative, *Chaos, Solitons Fractals* **22**, 907 (2004).
- [16] R. Metzler and J. Klafter, The restaurant at the end of the random walk: Recent developments in the description of anomalous transport by fractional dynamics, *J. Phys. A: Math. Gen.* **37**, R161 (2004).
- [17] S. Jespersen, R. Metzler, and H. C. Fogedby, Lévy flights in external force fields: Langevin and fractional Fokker-Planck equations and their solutions, *Phys. Rev. E* **59**, 2736 (1999).
- [18] R. Metzler and J. Klafter, From a generalized Chapman-Kolmogorov equation to the fractional Klein-Kramers equation, *J. Phys. Chem. B* **104**, 3851 (2000).
- [19] A. Chechkin, V. Gonchar, J. Klafter, R. Metzler, and L. Tanatarov, Stational states of non-linear oscillators driven by Lévy noise, *Chem. Phys.* **284**, 233 (2002).
- [20] M. Magdziarz and A. Weron, Fractional Fokker-Planck dynamics: Stochastic representation and computer simulation, *Phys. Rev. E* **75**, 016708 (2007).
- [21] A. V. Chechkin, V. Yu Gonchar, R. Gorenflo, N. Korabel, and I. M. Sokolov, Generalized fractional diffusion equations for accelerating subdiffusion and truncated Lévy flights, *Phys. Rev. E* **78**, 021111 (2008).
- [22] K. Gorska and K. Penson, Lévy stable two-sided distributions: Exact and explicit densities for asymmetric case, *Phys. Rev. E* **83**, 061125 (2011).
- [23] A. Kullberg and D. del-Castillo-Negrete, Transport in the spatially tempered, fractional Fokker-Planck equation, *J. Phys. A: Math. Theor.* **45**, 255101 (2012).
- [24] D. Reguera, P. Reimann, P. Hänggi, and J. M. Rubí, Interplay of frequency-synchronization with noise: Current resonance, giant diffusion and diffusion-crests, *Europhys. Lett.* **57**, 644 (2002).
- [25] L. Gammaitoni, P. Hänggi, P. Jung, and F. Marchesoni, Stochastic resonance, *Rev. Mod. Phys.* **70**, 223 (1998).
- [26] L. Gammaitoni, P. Hänggi, P. Jung, and F. Marchesoni, Stochastic resonance: A remarkable idea that changed our perception of noise, *Eur. Phys. J. B* **69**, 1 (2009).
- [27] Y. Kawamura, Collective phase dynamics of globally coupled oscillators: Noise-induced anti-phase synchronization, *Physica D* **270**, 20 (2014).
- [28] H. Kleinert, *Path Integrals in Quantum Mechanics, Statistics, Polymer Physics and Financial Markets* (World Scientific, Singapore, 2009).
- [29] D. del-Castillo-Negrete, B. A. Carreras, and V. E. Lynch, Nondiffusive Transport in Plasma Turbulence: A Fractional Diffusion Approach, *Phys. Rev. Lett.* **94**, 065003 (2005).
- [30] D. del-Castillo-Negrete, V. Yu. Gonchar, and A. V. Chechkin, Fluctuation-driven directed transport in the presence of Lévy flights, *Physica A* **387**, 6693 (2008).
- [31] R. J. Elliott and J. van der Hoek, A general fractional white noise theory and applications to finance, *Math. Finance* **13**, 301 (2003).
- [32] A. Cartea and D. del-Castillo-Negrete, Fractional diffusion models of option prices in markets with jumps, *Physica A* **374**, 749 (2007).
- [33] J. A. Roberts, T. W. Boonstra, and M. Breakspear, The heavy tail of the human brain, *Curr. Opin. Neurobiol.* **31**, 164 (2015).
- [34] Y. Kuramoto, *Chemical Oscillations, Waves and Turbulence* (Springer, Berlin, 1984).
- [35] L. DeVille, Transitions amongst synchronous solutions in the stochastic Kuramoto model, *Nonlinearity* **25**, 1473 (2012).
- [36] M. Freidlin and A. Wentzell, *Random Perturbations and Dynamical Systems*, 2nd ed. (Springer-Verlag, New York, 1998).
- [37] A. C. Kalloniatis and M. L. Zuparic, Fixed points and stability in the two-network frustrated Kuramoto model, *Physica A* **447**, 21 (2016).
- [38] A. Holder, M. Zuparic, and A. Kalloniatis, Gaussian noise and the two-network frustrated Kuramoto model, *Physica D* **341**, 10 (2017).
- [39] A. Kalloniatis and D. Roberts, Synchronisation of networked Kuramoto oscillators under stable Lévy noise, *Physica A* **466**, 476 (2017).
- [40] A. Kalloniatis and D. Roberts, Synchronisation under shocks: The Lévy Kuramoto model (unpublished).
- [41] R. Kawai and H. Masuda, On simulation of tempered stable random variates, *J. Comput. Appl. Math.* **235**, 2873 (2011).
- [42] A. Cartea and D. del-Castillo-Negrete, Fluid limit of the continuous-time random walk with general Lévy jump distribution functions, *Phys. Rev. E* **76**, 041105 (2007).

- [43] D. del-Castillo-Negrete, Anomalous transport in the presence of truncated Lévy flights, in *Fractional Dynamics: Recent Advances*, edited by J. Klafter, S. Lim, and R. Metzler (World Scientific, Singapore, 2012), pp. 129–157.
- [44] I. Podlubny, *Fractional Differential Equations* (Academic, San Diego, 1999).
- [45] S. Samko, A. Kilbas, and O. Marichev, *Fractional Integrals and Derivatives: Theory and Applications* (CRC, London, 1993).
- [46] K. Sato, *Lévy Processes and Infinitely Divisible Distributions* (Cambridge University Press, London, UK, 1999).
- [47] N. Berglund, B. Fernandez, and B. Gentz, Metastability in interacting nonlinear stochastic differential equations: I. From weak coupling to synchronization, *Nonlinearity* **20**, 2551 (2007).
- [48] R. Stratonovich, *Topics in the Theory of Random Noise* (Gordon and Breach, New York, 1967), Vol. III.
- [49] N. I. Fisher, *Statistical Analysis of Circular Data* (Cambridge University Press, Cambridge, UK, 1996).
- [50] H. Risken, *The Fokker-Planck Equation*, 2nd ed. (Springer, Heidelberg, 1989).